JGR Space Physics

RESEARCH ARTICLE
10.1029/2020JA028891

On the Association Between Electron Flux Oscillations and Local Phase Space Density Gradients

Theodore E. Sarris[1,2], Xinlin Li[2], Hong Zhao[2], Leng Ying Khoo[2], Wenlong Liu[3], and Michael A. Temerin[4]

[1]Department of Electrical and Computer Engineering, Democritus University of Thrace, Xanthi, Thrace, Greece, [2]Laboratory for Atmospheric and Space Physics, University of Colorado, Boulder, CO, USA, [3]School of Space and Environment, Beihang University, Beijing, China, [4]Retired from Space Sciences Lab, University of California Berkeley, Berkeley, CA, USA

Key Points:

- Amplitudes of drift-resonant electron flux oscillations associated with ultra-low frequency (ULF) waves are directly linked to phase space density gradients
- A flat radial phase space density profile leads to the disappearance of flux oscillations, even in the presence of ULF waves
- Combined knowledge of flux oscillations and phase space density could be used to assess the radial transport rates of energetic electrons

Correspondence to:
T. E. Sarris,
tsarris@ee.duth.gr

Citation:
Sarris, T. E., Li, X., Zhao, H., Khoo, L. Y., Liu, W., & Temerin, M. A. (2021). On the association between electron flux oscillations and local phase space density gradients. *Journal of Geophysical Research: Space Physics*, *126*, e2020JA028891. https://doi.org/10.1029/2020JA028891

Received 6 NOV 2020
Accepted 3 FEB 2021

Abstract Electron flux oscillations are often observed in electron energy channels in the range of 10 keV to 100 keV. They are observed in the form of flux fluctuations with periods corresponding to the drift periods of electrons around the Earth and can be produced in the magnetosphere as a result of drift resonant interactions in association with broadband ultra-low frequency (ULF) waves. They are observed in particular during quiet times and are indicators of ongoing drift-resonant processes and resulting radial transport caused by ULF waves. In this study we investigate the association of the appearance of such flux oscillations with the local phase space density. In particular, it is shown that flux oscillations appear when nonzero phase space density gradients are present and furthermore that the observed amplitude of flux oscillations is dependent on radial phase space density gradients, with steeper gradients enabling the observation of flux oscillations with higher-amplitude. Via statistical observations from the Van Allen probes twin-spacecraft mission while at apogee at L^* ~5 to ~5.6 it is found that, during quiet times, electron flux oscillations are more likely to diminish for electron energy of ~400 keV, and associated phase space density is more likely to be zero for the corresponding first adiabatic invariant values of ~300 MeV/G. It is also concluded that flux oscillations could be used as indicators of phase space density gradients.

1. Introduction

In studying magnetospheric processes, monitoring the derived phase space densities (PSD) of electrons at constant adiabatic invariants is often preferred over the direct monitoring of electron flux along spacecraft orbits (e.g., Chen et al., 2006). Electron flux $j(\vec{r}, t, E, \alpha)$, measured at a spacecraft location $(\vec{r})$ at a certain time (t) as a function of energy (E) and local pitch angle (α), is converted to PSD $f(\mu, K, L^*, t)$ by restricting measurements to only electrons with energy and pitch angle corresponding to fixed values of the three adiabatic invariants μ, K, and L^* (Roederer, 1970; Roederer & Zhang, 2014); thus the transformation requires calculating the three invariants along the spacecraft orbit (e.g., Chen et al., 2005; Hilmer et al., 2000). In the following we describe PSD in terms of the L^* parameter, which is the radial distance on the equatorial plane where an electron would be located if all external magnetic fields were slowly turned off, leaving only the internal dipole field (see, e.g., Green & Kivelson, 2004). Monitoring PSD in terms of L^* has the advantage that it can help separate adiabatic effects (such as the Dst effect; see, Kim & Chan, 1997; Li et al. 1997) from nonadiabatic ones; it also helps to relate electron flux measurements made at different regions of the magnetosphere.

Related to ULF wave-induced radial diffusion and transport, the radial diffusion equation dictates that electron populations on average are transported via diffusion from drift shells with larger PSD to drift shells with smaller PSD (Schulz & Lanzerotti, 1974); hence knowledge of the local PSD gradient is essential in quantifying the effectiveness of ULF waves in radially transporting electrons inwards or outwards. The dependence of the phase space density gradients on μ, with positive gradients observed at lower μ, negative at higher μ and with a flat transition around 300 MeV/G near the geosynchronous orbit (GEO), has been noted by several studies, based on measurements from LANL geosynchronous spacecraft, the THEMIS constellation, and the Van Allen Probes; these include the studies by Li et al. (1993), (1999), (2003), Turner and Li (2008), Turner et al. (2012), Boyd et al. (2014).

Several studies have reported the appearance of 100 keV electron flux oscillations at the drift frequency of electrons around the Earth, modulated by ULF waves (e.g., Claudepierre et al., 2013; Hudson et al., 2020; Zong et al., 2007). Furthermore, Su et al. (2015) presented an event where highly relativistic electron fluxes were modulated by ULF waves throughout the outer radiation belt for about 10 hours, serving as evidence for the global and long-lasting drift resonant interaction between ULF waves and relativistic electrons. In Sarris et al. (2020), it was demonstrated through particle-tracing simulation and observations from the Magnetic Electron Ion Spectrometer (MagEIS), (Blake et al., 2013) onboard the Van Allen Probes, that periodic flux oscillations of hundreds-keV are often observed in the magnetosphere, in particular during quiet times. Such flux oscillations are not necessarily associated with drift-periodic oscillations that accompany energetic particle injections following storms or substorms, termed drift echoes (Lanzerotti et al., 1967), as their amplitudes remain elevated over subsequent passes by the Van Allen Probes, whereas the amplitudes of drift echoes following storm- or substorm-related injections gradually diminish. Instead, they can be linked to the resonant interaction of electrons with ULF waves and, as discussed in Sarris et al. (2020), they could be used as an indicator of electron radial diffusion. It was demonstrated that critical in the observations of flux oscillations is the width of electron detector energy channels, with narrower energy channels enabling the detection of flux oscillations of smaller amplitude. The underlying principle is that, for a finite energy range of each channel, electrons with different energies and drift periods within this channel will partially phase mix over a few drift periods, obscuring the amplitude of flux oscillations for appearing. In that study, the effects of different energy widths were investigated and quantified through particle tracing simulations via a parametric study that introduced different energy channels in a virtual detector in the simulation and results were confirmed using the ultra-high energy-resolution data of MagEIS. The significance of energy channel resolutions on the study of ULF waves interactions with ∼1 MeV electrons was also highlighted by Hartinger et al. (2018).

The relation between flux oscillation amplitudes on the local PSD gradient was demonstrated via test-particle simulations in broadband ULF waves in Sarris et al. (2017). This can be understood as follows: under the effect of ULF waves, particles can either be transported inwards or outwards; however if the local PSD profile at the location of observation has a net zero radial gradient, then relatively constant fluxes would be observed as particles are transported radially inwards or outwards while preserving the first adiabatic invariant. Similarly, a smaller (larger) PSD gradient would lead to smaller (larger) flux oscillations. Furthermore, Hartinger et al. (2020) have recently shown that the expected drift resonance response of electrons close to geostationary orbit can be masked by small radial PSD gradients, which could explain the relatively small number of past studies reporting the drift resonance of >∼1 MeV electrons; they also argued that observations of the radial PSD profile should also be included in studies aiming at characterizing radial transport processes via drift resonance.

Expanding on these past studies, in this study we explore the prediction that often the flux oscillations might be weak at energies in the several hundred keV range near GEO due to PSD gradients often being flat. We present statistical observations of electron flux oscillation at locations around the apogee of the Van Allen Probes, at an L^* range from 5 to 5.6, and we investigate the PSD gradients at various μ values corresponding to the energy channels of the MagEIS instrument. For the calculation of L^* the TS04 magnetic field model is used (Tsyganenko & Sitnov, 2005). We show that a nonzero PSD spatial gradient as a function of L^* is required for the observation of electron flux oscillations, and, inversely, that the appearance of flux oscillations in some energy channels together with the lack of flux oscillations in other energy channels is an indication of a flat PSD for the channels where oscillations are not observed.

2. Observations of Electron Flux Oscillation Observations and PSD Gradients

In Figure 1 we present one representative event of observations of flux oscillations on March 11, 2013, as observed by MagEIS during an apogee pass of Van Allen Probe B. During this apogee pass, oscillations in electron fluxes are observed in most energy channels from ∼30 keV–700 keV. The frequencies of these oscillations closely match the average drift frequencies of electrons within each channel. This event was used in Sarris et al. (2020) to parameterize test-particle simulations under the effect of ULF waves that reproduced the observed flux oscillations in lower energy channels and demonstrated the effect of energy channel width on flux oscillation amplitudes. In this figure we can observe that energy channel of 339 keV (and, to

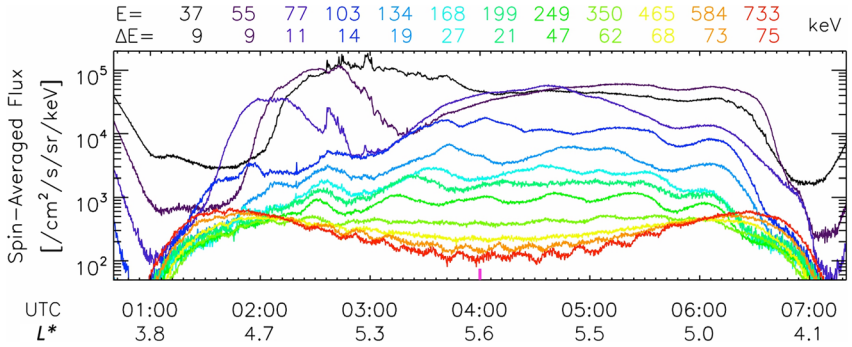

Figure 1. MagEIS electron fluxes as a function of universal time and L^* on March 11, 2013, during an apogee pass of Van Allen Probe (b) Energy channels and corresponding widths in energy are shown in the top of the plot. The time when the s/c is located at apogee is indicated with a purple mark in the lower part of the plot. L^*, adiabatic invariant; MagEIS, Magnetic Electron Ion Spectrometer.

a lesser degree, that of 459 keV) show little or no fluctuation, whereas both lower energy channels (235 keV and below) and higher energy channels (584 keV and above) clearly show oscillations of higher amplitudes.

To demonstrate the effect of local PSD gradients on the amplitude of these flux oscillations, we first calculate the values of μ that correspond to the MagEIS energy channels when Van Allen Probes were located at apogee. Subsequently, in Figure 2 we plot the estimated PSD profiles as a function of L^* on March 11, 2013, for the calculated μ-values. These μ-values are listed next to each PSD profile, and the corresponding energy channel of the MagEIS instrument when Van Allen Probe-B was located at apogee is also listed in parenthesis. The color code used for the PSD values at each μ-value is the same as the color code for the corresponding MagEIS energy channel when the Van Allen Probe is located at apogee, and the same color indications will be used throughout this study for the energy values in parentheses and the corresponding PSD values. A black frame around outer L^*-values marks the range of L^*-values that were used to estimate the spatial gradients of PSD, and also the region where the corresponding flux oscillations are investigated.

We note that, indeed, close to the apogee of Van Allen Probe-B there is a change in the slope of the PSDs around the μ-value of 314 MeV/G that corresponds to the 339 keV energy channel at apogee: higher μ-values

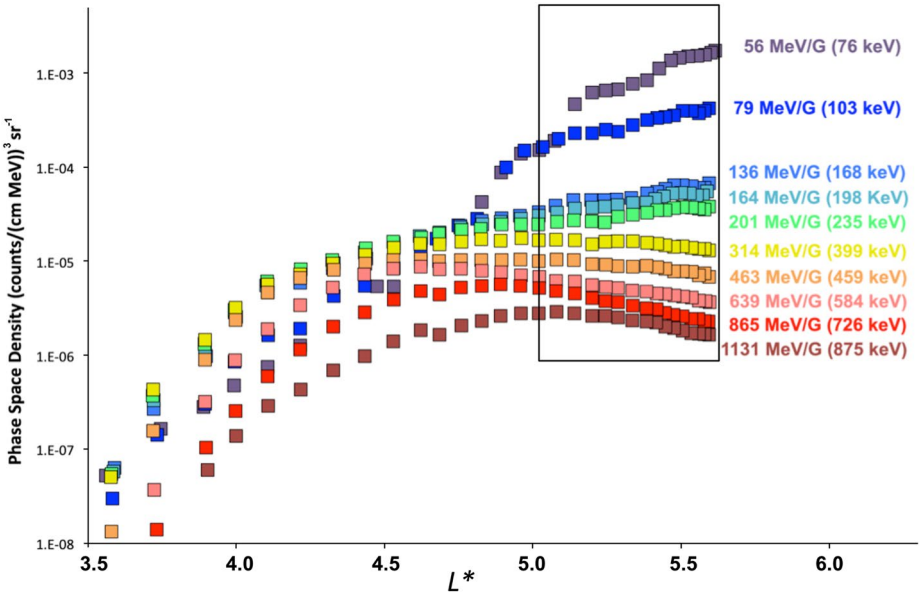

Figure 2. Phase Space Density as a function of L^*, for the average μ-values that correspond to the various MagEIS energy channels at Van Allen Probe apogee from $L^* = 5$ to 5.6, as marked. L^*, μ, adiabatic invariant; MagEIS, Magnetic Electron Ion Spectrometer.

have an outward-negative slope whereas lower μ-values have an outward-positive slope. Such change in the slope of the PSD gradients across different μ-values at outer L^* has been noted by Li et al. (2014); in their study they plotted electron PSD from March 16 to 19 for three μ-values (200 MeV/G, 400 MeV/G, and 1,000 MeV/G) and commented that the dynamics for lower μ electrons can be better explained by radial diffusion, while for higher μ electrons local acceleration processes become important, in particular following the strong March 17–18, 2013 event. In addition, through a statistical study based on MMS-1 data from January 2017 to December 2018, Liu et al. (2020) investigated the radial gradient of L^* and identified that crossover μ, defined as the μ-value at which PSD radial gradient is equal to 0, stays relatively constant at $\mu \sim$300 MeV/G inside $L^* \sim 6$, but decreases as L^* increases outside $L^* \sim 6$. They attributed the resulting distribution patterns of PSD in L^* to the interplay between injections from the magnetotail, loss of electrons through the magnetopause at outer L^* and local acceleration.

It is also noted that if the flux oscillations were coherent responses to a monochromatic external perturbation, then the flux oscillations across the energy channel corresponding to zero PSD gradient would be phase-shifted by 180°: an increase in flux at a low energy channel below 339 keV would be in-phase with a decrease in flux at a higher energy channel above 339 keV, whereas, as noted above, the 339 keV energy channel would show no variation. However, in this event, as demonstrated in Sarris et al. (2020), the flux oscillations are drift-resonant responses to broadband flux oscillations, and the phases of the fluctuations in each energy channel cannot be cross-compared across the different energy channels.

In the following we investigate the dependence of the amplitude of the flux oscillations on the PSD gradient. We calculate the absolute value of the PSD gradients at each μ-value for PSD estimates within a distance of $\Delta L^* = 0.6$ from apogee. PSD gradients are estimated by performing linear fits to the values of PSD versus L^*. The calculated linear fits are plotted in Figure 3, together with the corresponding equations showing the estimated slopes of the fits and their R^2 values, which is a measure of the goodness-of-fit for linear regression models. Similarly to Figure 2, for $\mu = 314$ MeV/G the calculated linear fit is approaching a horizontal line, marking the transition from outwards positive gradients for lower μ-values to outwards negative gradients for outwards negative μ-values; the estimation of R^2 is omitted for $\mu = 314$ MeV/G, since a linear regression is not the optimal measure of goodness-of-fit in the case of close-to-horizontal lines, however a linear fit appears to be good in this case too.

It is noted that the data used in estimating PSD in Figure 3 are obtained from both the outbound and inbound segments of the Van Allen Probe B orbit and might thus include time-dependent effects that are not taken into account when calculating the PSD versus L^* profiles. In addition sampling along the outbound and inbound passes occurs naturally at different local times, and local time dependence is also not investigated in this study. Investigating the spatial structure and temporal evolution would require multispacecraft measurements in formations such as have been used, for example, in the study by Liu et al. (2011) in the context of ULF wave events.

Subsequently, the relative amplitudes of flux oscillations for each channel corresponding to the μ-value of each PSD value are plotted as a function of the absolute value of the gradient of the linear fit. Here, as relative flux oscillation amplitude we define the amplitude of the oscillations in the de-trended fluxes divided by the average value of the de-trended flux at apogee, within the same range of L^* as plotted above ($L^* = 5$ to 5.6), and is dimensionless. The values of the relative amplitude versus PSD gradient for all energy channels considered are plotted in Figure 4.

The color-coding in Figure 4 indicates the μ-values for which PSD gradients are calculated and is the same as the color-coding of the PSD in Figures 2 and 3 and of the color-code of the energy channel corresponding to these PSD profiles at Van Allen Probes' apogee as plotted in Figure 1. The black line indicates the least squares fitting of a curve through these μ-values, plotted so as to indicate the relationship between the flux oscillation amplitude and PSD gradient during this specific pass. We observe that the flux oscillation amplitudes as calculated from fluxes at the various channels are directly related to the PSD gradients, with larger gradients generally leading to larger flux oscillation amplitudes. The fitted function in this plot indicates a power-law dependence. We note however that, as discussed in Sarris et al. (2020), the dependence on energy channel width is also included in these observations, and that de-coupling the two factors on which the flux oscillation amplitudes depend need a further detailed parametric study, as discussed below. In addition, it

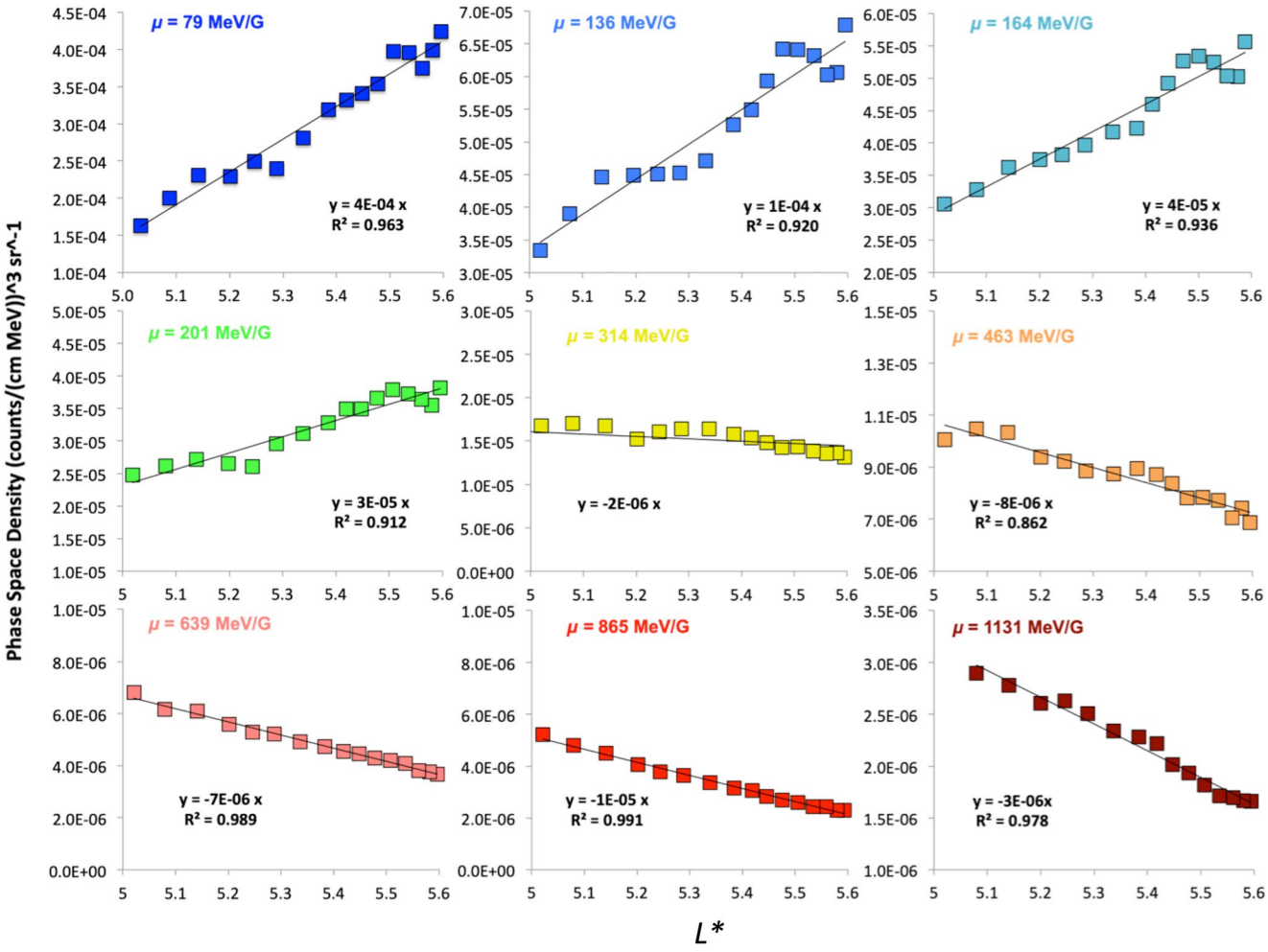

Figure 3. Linear fits through all PSDs estimated within $\Delta L = 0.6$ from apogee. The equations of the linear fits and corresponding R^2 values are also plotted. Colors correspond to the μ-values of Figure 2. μ, adiabatic invariant; PSDs, phase space densities.

is noted that the relation between relative flux oscillation amplitude and PSD gradient is event-specific, and that comparing between different events is not straight forward, even for subgroups of events where the PSD gradient appears to be zero for the same energy channel; this is due to the expected dependence of flux oscillation amplitudes on the electric and magnetic field ULF fluctuations and PSD gradients, as discussed also in the conclusions. We also note that the absolute values of the PSD gradients for higher μ-values, marked with orange, light-red and red squares actually correspond to negative outward slopes and that, as discussed above, these would correspond to anticorrelated flux oscillations with respect to lower μ-values if the oscillations were coherent.

3. Statistical Analysis

A statistical ensemble of events is accumulated for which flux oscillations are observed in at least some of the lower energy channels. It is noted that no events were identified where flux oscillations appear in all MagEIS energy channels. A total of 120 events is selected for the statistical analysis in the period from October 2012 until October 2014. The events are selected based on the following criteria: (1) electron flux oscillations are observed in at least one of the Van Allen Probes' MagEIS energy channels, from 54 keV to ~1 MeV, at frequencies that correspond to the characteristic drift-frequency of electrons within each energy channel; (2) flux oscillations are observed for at least 2 hours around Van Allen Probes' apogee, so that multiple drift periods can be identified; (3) there are no evident dispersionless particle injections prior to

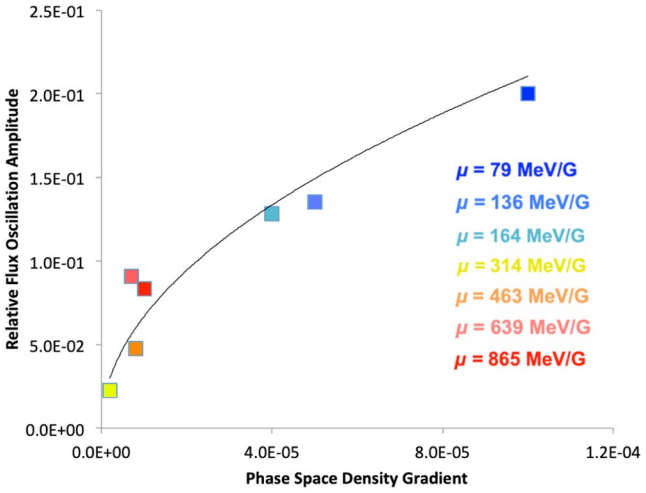

Figure 4. Values of the relative flux oscillation amplitude as a function of PSD gradient. Colors correspond to the μ-values of Figure 3 and also to the corresponding energy channels of these μ-values at the Van Allen Probes' apogee. PSD, phase space density; μ, adiabatic invariant.

the flux oscillations, such that could be associated, for example, with substorm injections, which are also known to cause periodic flux oscillations in the form of drift-echoes. It is noted that these events pertain primarily to quiet geomagnetic conditions, as continuous flux oscillation events are more easily identified during these times; subsequent studies during active times with signal processing algorithms that enable extracting the amplitude of flux oscillations at the drift frequency range of each energy channel could help expand the statistics and reveal the dependence of flux oscillations to solar wind conditions.

Subsequently, for each of the 120 flux oscillation events, the energy channel where flux oscillations stop being evident is identified and events are classified accordingly based on this energy channel. The classification of the total number of 120 flux oscillation events according to this scheme is presented in Figure 5, normalized per total number of events (percentage of events). In this figure, color-coded is the energy of the various energy channels according to the color scheme of Figure 1. Thus, for a given energy channel corresponding to any black dot along the black curve, all lower energy channels below this energy channel would show flux oscillations. The lack of events for the four first energy channels of 36, 54, 76, and 103 keV (four first black dots for lowest energies) indicates that there are no events where flux oscillations are observed in a lower energy channel, but are not observed in these four first energy channels; for example, the bin at 103 keV indicates that there are no events where flux oscillations are observed in either the 36, 54, or 76 keV energy channels, but disappear in the 103 keV channel. Three example events are plotted in the lower thee panels of Figure 5, marked as A, B, and C for which flux oscillations are observed in all energy channels lower

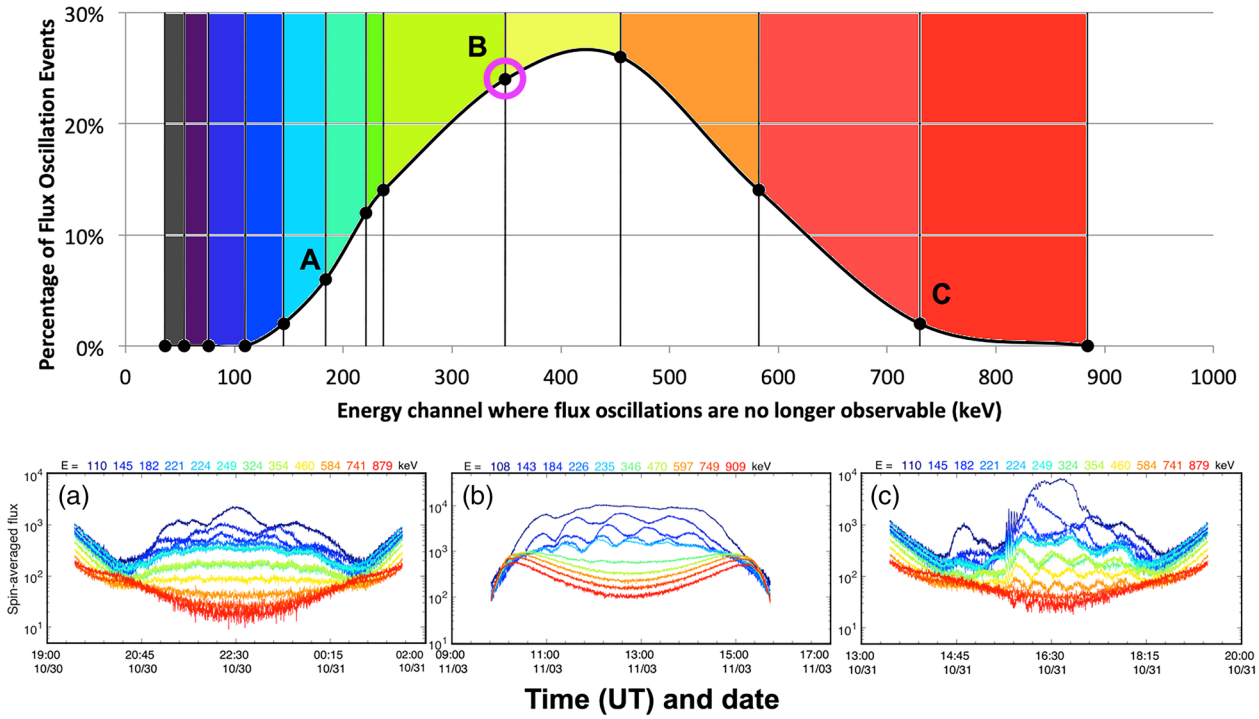

Figure 5. Top panel: Percentage of occurrences of events where flux oscillations are observed in lower energy channels when the Van Allen Probes are located at apogee but are not observed in the energies marked by the horizontal axis. All events used in obtaining the statistical distribution of this figure are based on observations of flux oscillations at lower energy channels and a lack of observations at higher energies. Three example events are plotted in the lower panels corresponding to bins A, B, and C, as marked.

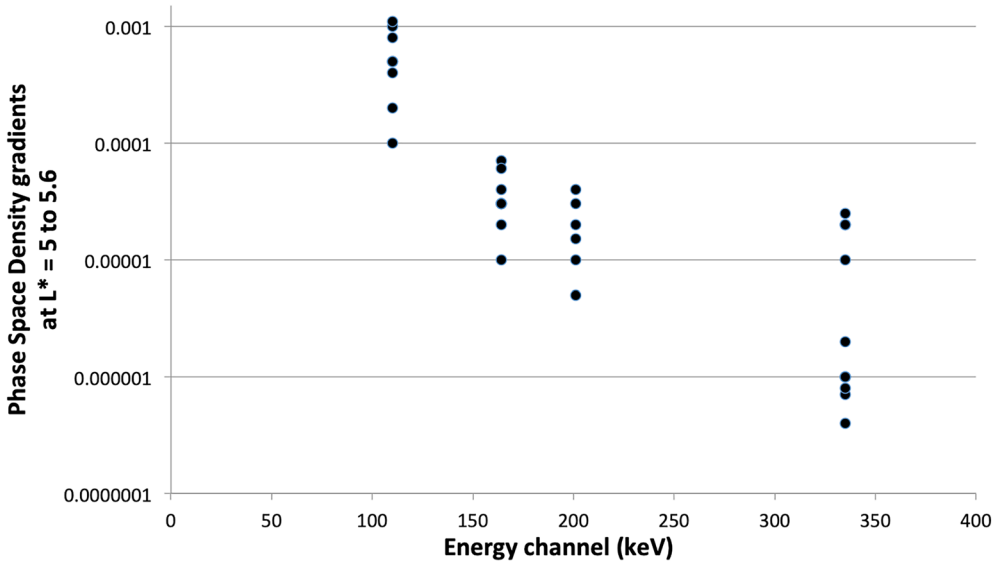

Figure 6. Phase Space Density gradients, in units of (counts/(cm MeV))^3 sr^{-1}, in the *L** range from 5 to 5.6, for flux oscillation events where oscillations are observed in lowest energy channels up to 346 keV (excluding). *L**, adiabatic invariant.

than 184, 346, and 730 keV, respectively. The events B that are also marked with a purple circle are further analyzed statistically in the following.

Subsequently, the radial gradients of PSD as a function of *L** are calculated for each event by performing a linear fit to PSD values for *L** range from 5 to 5.6, similarly to the example shown in Figure 3. The results of PSD gradients for all events where flux oscillations were observed in all energy channels lower than 346 keV energy channel (marked in a purple circle in Figure 5) are presented in Figure 6.

In the above plot it is observed that, for the selected events where flux oscillations are observed in the lower energy channels when the Van Allen Probes are located at perigee but are not observed in 346 keV, PSD gradients are steeper in lower energies and are gradually diminishing at energies where flux oscillations are not observed. Thus, whereas flux oscillations are a common feature in the radiation belts, they are most often observed in the lowest energy channels, as at higher energy channels the corresponding PSD gradients are often close to zero in the *L** range from 5 to 5.6. It can also be seen that flux oscillations are closely linked to the local gradient of PSD and could thus be used as indicators of the local PSD gradients.

4. Discussion and Conclusions

We have demonstrated through the Van Allen Probe's MagEIS observations that electron flux oscillations at the electron drift frequency are closely linked to the local PSD gradient, with larger gradients (either positive or negative) leading to larger flux oscillation amplitudes, and zero gradients (flat PSDs) leading to no flux oscillations being observed. This is a typical pattern for the majority of events, in that flux oscillations are observed with higher amplitudes in the lowest energy channels and that amplitudes gradually diminish for higher energies. It has been shown that in the above classification the energy channel where flux oscillations disappear also indicates the μ-value where PSD gradients are expected to be zero. The statistical analysis of a large number of flux-oscillation events identified around Van Allen Probes' apogee indicates that most commonly flux oscillations are observed in energy channels below 400 keV; in the *L** range between 5 and 5.6 this corresponds to a μ-value of 314 MeV/G, and it is these μ-values where we would expect a flat PSD. This is consistent with the observations in the statistical study by Liu et al. (2020), who indicate that crossover μ at which PSD radial gradient is equal to 0, is most commonly ~300 MeV/G inside *L** ~6. Thus, flux oscillations can also be used as indicators of the local gradient of PSD, by observing the relative amplitude of oscillations at various μ-values. The quantification of the relationship of the relative amplitude of oscillations is the subject of a future study.

It is noted that other parameters are also important in the resulting amplitudes of flux oscillation, such as the effects of the energy width of electron detector channels (Sarris et al., 2020) as well as the power of ULF waves and its distribution in azimuthal wavenumbers (Sarris et al., 2013; Sarris and Li, 2017). For example, it is noted that in Figure 6 PSD gradients statistically do not reach a value of zero for energy channels where flux oscillations are not observed. This is possibly due to the larger width of higher energy channels, as discussed in Sarris et al. (2020), or to weaker ULF wave power at the corresponding frequencies.

The above parameters are all coupled, and a detailed parametric study via particle tracing simulations would be required to describe and quantify the dependence of flux oscillation amplitudes simultaneously on the energy widths of electron detectors, on the local gradients of PSD and on the power of ULF waves. For a given electron detector energy width, this parametric study can include particle-tracing simulations under measured PSD gradients and ULF wave power that manages to reproduce the flux oscillation amplitudes at all energy channels. Subsequent simulations by varying the PSD gradients and for varying levels of ULF wave power would help yield the effects on the resulting flux oscillation amplitudes. This could lead to an empirical relationship that predicts the appearance and amplitudes of such flux oscillations, taking into account the dependence on all the above factors, for example, by performing fits such as demonstrated in Figure 4. Inversely, if simultaneous observations of flux oscillations and PSD gradients are available, this could lead to estimates of the ULF wave power that is required to produce the observed fluctuations.

Data Availability Statement

Van Allen Probes data used in this manuscript are in the public domain and accessible from the Van Allen Probes Science Gateway https://cdaweb.sci.gsfc.nasa.gov/. Van Allen Probes PSD data are publicly available at http://rbspgway.jhuapl.edu/psd.

Acknowledgments
This work was supported in part by the National Science Foundation under Grant No.1952903, by NASA grants NNX15AF56G and NNX17AD85G and by NASA/RBSP-ECT and -EFW funding through JHU/APL Contract 967399 under prime NASA Contract NAS5-01072 (Van Allen Probes), and NASA Contract NAS5-02099 (THEMIS).

References

Blake, J. B., Carranza, P. A., Claudepierre, S. G., Clemmons, J. H., Crain, W. R., Jr., Dotan, Y., et al. (2013). The magnetic electron ion spectrometer (MagEIS) instruments aboard the radiation belt storm probes (RBSP) spacecraft. *Space Science Reviews*, *179*, 383–421. https://doi.org/10.1007/s11214-013-9991-8

Boyd, A. J., Spence, H. E., Claudepierre, S. G., Fennell, J. F., Blake, J. B., Baker, D. N., et al. (2014). Quantifying the radiation belt seed population in the 17 March 2013 electron acceleration event. *Geophysical Research Letters*, *41*, 2275–2281. https://doi.org/10.1002/2014GL059626

Roederer, J. G., & Zhang, H. (2014). *Dynamics of magnetically trapped particles* (2nd ed.). New York: Springer. Retrieved from https://doi.org/10.1007/978-3-642-41530-2

Chen, Y., Friedel, R. H. W., & Reeves, G. D. (2006). Phase space density distributions of energetic electrons in the outer radiation belt during two Geospace Environment Modeling Inner Magnetosphere/Storms selected storms. *Journal of Geophysical Research: Space Physics*, *111*, A11S04. https://doi.org/10.1029/2006JA011703

Chen, Y., Friedel, R. H. W., Reeves, G. D., Onsager, T. G., & Thomsen, M. F. (2005). Multisatellite determination of the relativistic electron phase space density at geosynchronous orbit: Methodology and results during geomagnetically quiet times. *Journal of Geophysical Research*, *110*, A10210. https://doi.org/10.1029/2004JA010895

Claudepierre, S. G., Mann, I. R., Takahashi, K., Fennell, J. F., Hudson, M. K., Blake, J. B., et al. (2013). Van Allen Probes observation of localized drift resonance between poloidal mode ultra-low frequency waves and 60 keV electrons. *Geophysical Research Letters*, *40*, 4491–4497. https://doi.org/10.1002/grl.50901

Green, J. C., & Kivelson, M. G. (2004). Relativistic electrons in the outer radiation belt: Differentiating between acceleration mechanisms. *Journal of Geophysical Research*, *109*, A03213. https://doi.org/10.1029/2003JA010153

Hartinger, M. D., Claudepierre, S. G., Turner, D. L., Reeves, G. D., Breneman, A., Mann, I. R., et al. (2018). Diagnosis of ULF wave-particle interactions with megaelectron volt electrons: The importance of ultrahigh-resolution energy channels. *Geophysical Research Letters*, *45* 11883–11892. https://doi.org/10.1029/2018GL080291

Hartinger, M. D., Reeves, G. D., Boyd, A., Henderson, M. G., Turner, D. L., Komar, C. M., et al. (2020). Why are there so few reports of high energy electron drift resonances? Role of radial phase space density gradients. *Geophysical Research Letters*, *12*(8), e2020JA027924. https://doi.org/10.1029/2020JA027924

Hilmer, R. V., Ginet, G. P., & Cayton, T. E. (2000). Enhancement of equatorial energetic electron fluxes near L = 4.2 as a result of high speed solar wind streams. *Journal of Geophysical Research*, *105*(A10), 23311–23322. https://doi.org/10.1029/1999JA000380

Hudson, M. K., Elkington, S. R., Li, Z., & Patel, M. (2020). Drift echoes and flux oscillations: A signature of prompt and diffusive changes in the radiation belts. *Journal of Atmospheric and Solar-Terrestrial Physics*, *207*, 105332. https://doi.org/10.1016/j.jastp.2020.105332

Kim, H.-J., & Chan, A. A. (1997). Fully adiabatic changes in storm time relativistic electron fluxes. *Journal of Geophysical Research*, *102*, 22107–22116. https://doi.org/10.1029/97JA01814

Lanzerotti, L. J., Roberts, C. S., & Brown, W. L. (1967). Temporal variations in the electron flux at synchronous altitudes. *Journal of Geophysical Research*, *72*(23), 5893–5902. https://doi.org/10.1029/JZ072i023p05893

Li, X., Baker, D. N., Elkington, S., Temerin, M., Reeves, G. D., Belian, R. D., et al. (2003). Energetic particle injections in the inner magnetosphere as a response to an interplanetary shock. *Journal of Atmospheric and Solar Terrestrial Physics*, *65*, 233–244. https://doi.org/10.1016/S1364-6826(02)00286-9

Li, X., DN Baker, M. T., Cayton, T. E., Reeves, E. G. D., Christensen, R. A., Blake, J. B., et al. (1997). Multisatellite observations of the outer zone electron variation during the November 3–4, 1993, magnetic storm. *Journal of Geophysical Research*, *102*(A7), 14123–14140. https://doi.org/10.1029/97JA01101

Li, X., DN Baker, M. T., Cayton, T. E., Reeves, G. D., Selesnick, R. S., Blake, J. B., et al. (1999). Rapid enhancements of relativistic electrons deep in the magnetosphere during the May 15, 1997, magnetic storm. *Journal of Geophysical Research*, *104*(A4), 4467–4476. https://doi.org/10.1029/1998JA900092

Li, W., Thorne, R. M., Ma, Q., Ni, B., Bortnik, J., Baker, D.N., et al. (2014). Radiation belt electron acceleration by chorus waves during the 17 March 2013 storm. *Journal of Geophysical Research: Space Physics*, *119*, 4681–4693. https://doi.org/10.1002/2014JA019945

Li, X., Roth, I., Temerin, M., Wygant, J. R., Hudson, M. K., & Blake, J. B. (1993). Simulation of the prompt energization and transport of radiation belt particles during the March 24, 1991 SSC, *Geophysical Research Letter*, *20*, 2423–2426. https://doi.org/10.1029/93GL02701

Liu, W., Sarris, T. E., Li, X., Zong, Q.-G., Ergun, R., Angelopoulos, V., et al. (2011). Spatial structure and temporal evolution of a dayside poloidal ULF wave event. *Geophysical Research Letters*, *38*, L19104. https://doi.org/10.1029/2011GL049476

Liu, Z.-Y., Zong, Q.-G., & Blake, J. B. (2020). On phase space density and its radial gradient of outer radiation belt seed electrons: MMS/FEEPS observations. *Journal of Geophysical Research: Space Physics*, *125*, e2019JA027711. https://doi.org/10.1029/2019JA027711

Roederer, J. G. (1970). *Dynamics of geomagnetically trapped radiation*. 14, (p. 166). New York: Cambridge University Press. Retrieved from https://www.springer.com/gp/book/9783642493027

Sarris, T. E., Li, X., Liu, W., Argyriadis, E., Boudouridis, A., & Ergun, R. (2013). Mode number calculations of ULF field-line resonances using ground magnetometers and THEMIS measurements. *Journal of Geophysical Research: Space Physics*, *118*, 6986–6997. https://doi.org/10.1002/2012JA018307

Sarris, T. E., Li, X., Temerin, M., Zhao, H., Califf, S., Liu, W., et al. (2017). On the relationship between electron flux oscillations and ULF wave-driven radial transport. *Journal of Geophysical Research: Space Physics*, *122*. https://doi.org/10.1002/2016JA023741

Sarris, T. E., Li, X., Temerin, M., Zhao, H., Khoo, L. Y., Turner, D. L., et al. (2020). Simulations of electron flux oscillations as observed by MagEIS in response to broadband ULF waves. *Journal of Geophysical Research: Space Physics*, *125*, e2020JA027798. https://doi.org/10.1029/2020JA027798

Schulz, M., & Lanzerotti, L. (1974). *Particle diffusion in the radiation belts*. (pp. 153–159). New York: Springer. Retrieved from https://www.springer.com/gp/book/9783642656774

Su, Z., Zhu, H., Xiao, F., Zong, Q.-G., Zhou, X.-Z., Zheng, H., et al. (2015). Ultra-low-frequency wave-driven diffusion of radiation belt relativistic electrons. *Nature Communications*, *6*, 10096. https://doi.org/10.1038/ncomms10096

Tsyganenko, N. A., & Sitnov, M. I. (2005). Modeling the dynamics of the inner magnetosphere during strong geomagnetic storms. *Journal of Geophysical Research*, *110*, A03208. https://doi.org/10.1029/2004JA010798

Turner, D. L., Angelopoulos, V., Shprits, Y., Kellerman, A., Cruce, P., & Larson, D. (2012). Radial distributions of equatorial phase space density for outer radiation belt electrons. *Geophysical Research Letters*, *39*, L09101. https://doi.org/10.1029/2012GL051722

Turner, D. L., & Li, X. (2008). Radial gradients of phase space density of the outer radiation belt electrons prior to sudden solar wind pressure enhancements. *Geophysical Research Letters*, *35*, L18101. https://doi.org/10.1029/2008GL034866

Zong, Q., Zhou, X.-Z., Li, X., Song, P., Fu, S. Y., Baker, D. N., et al. (2007). Ultralow frequency modulation of energetic particles in the dayside magnetosphere. *Geophysical Research Letters*, *34*, L12105. https://doi.org/10.1029/2007GL029915